Acta Cryst. (1981). A**37**, 876–889

Simultaneous Bragg Diffraction of X-rays from Liquid-Phase Epitaxial Thin Films

BY SHIH-LIN CHANG*

Instituto de Física 'Gleb Wataghin', Universidade Estadual de Campinas, Campinas 13100-1170, *São Paulo, Brazil*

(*Received* 9 *October* 1980; *accepted* 12 *May* 1981)

Abstract

Multiple simultaneous Bragg diffraction effects of X-rays in quaternary III–V liquid-phase epitaxial thin layers are investigated with both photographic and counter detection methods. For the photographic investigation, a divergent source is used. The geometric aspects of this type of diffraction, affected by lattice mismatch between epitaxial layers and substrates, are discussed for cases involving five-, six- and eight-beam reflections. The lattice mismatches in directions parallel and perpendicular to the interface normal of InGaAsP/InP, determined from a single divergent-beam photograph, are obtained. For the counter detection study, a collimated incident beam and several single and double heterojunction samples, with large lattice mismatches are used. A kinematical treatment for a general *n*-beam diffraction, from double- and triple-layer systems, is derived to account for the measured intensities.

Introduction

Although the photographic investigation and the counter detection of multiple X-ray diffraction effects in single crystals were reported in the late 1930's by Kossel (1936) and Renninger (1937), respectively, simultaneous Bragg diffraction did not receive proper attention until about 1960. Since then, extensive studies on this subject have been carried out by many investigators. These include Cole, Chambers & Dunn (1962), Moon & Shull (1964), Zachariasen (1965), Caticha-Ellis (1969), Prager (1971), Post (1975*b*), Unangst & Melle (1975), Hess (1975), Cousins, Gerward & Staun Olsen (1978) and many others. All these works were devoted to the discussion of the geometry and the intensities of simultaneous Bragg diffraction effects in bulk single crystals. No investigations have been made on these effects in epitaxial thin films. In this article we report our investigations on the geometry and intensity aspects of simultaneous Bragg diffraction effects in III–V liquid-phase epitaxial (LPE) thin films.

The samples under study in this paper are $In_{1-x}Ga_xAs_yP_{1-y}$ LPE thin films deposited on an InP substrate, where x and y are gallium and arsenic concentrations in the solid composition, respectively. InGaAsP materials are usually in the form of single crystals. Their lattice constants vary with the gallium and arsenic concentrations, X^l_{Ga} and X^l_{As} in the liquid phase, or the corresponding x and y concentrations in the solid phase. The growth conditions and characterizations of InGaAsP/InP heterojunctions can be obtained from the articles of Antypas & Moon (1973) and Nakajima, Kusunoki, Akita & Kotani (1978). Two experiments were carried out. One used the high-resolution divergent-beam method (Chang, Patel, Nannichi & Prince, 1979) to show how multiple diffraction images vary with small lattice mismatch between the epitaxial thin layer and substrate. Samples of single hetero-junction (SH) with small lattice mismatch were employed. The other experiment used a collimated incident beam and a detector to measure the reflected intensities of multiple diffractions from single (SH) and double heterojunction (DH) samples. The lattice mismatches of these samples were one order of magnitude higher than those for the divergent-beam experiment. Based on Moon & Shull's (1964) treatment, a kinematical theory for multiple X-ray diffractions from multi-layer systems was derived to account for the measured intensities.

According to Oe, Shinoda & Sugiyama (1978), [001] InGaAsP materials possess tetragonal unit cells owing to small differences between $\Delta a_\perp$ and $\Delta a_\parallel$. $\Delta a_\perp$ and $\Delta a_\parallel$ are equal to $a_\perp - a_s$ and $a_\parallel - a_s$, where a_s, $a_\perp$ and $a_\parallel$ are the lattice constants of the InP substrate and of the epi-layer in the directions normal and parallel to the interfacial plane. The geometry in reciprocal-lattice space of simultaneous Bragg diffractions is then affected by $\Delta a_\parallel$ and $\Delta a_\perp$. This is discussed below in comparison with the InP cubic cases.

* On leave at the Max-Planck-Institut für Festkörperforschung, Stuttgart, Federal Republic of Germany, from March 1981 to February 1982.

0567-7394/81/060876-14$01.00

© 1981 International Union of Crystallography

Geometry

Multiple diffraction occurs when several reciprocal-lattice points are simultaneously brought onto the surface of the Ewald sphere to diffract an incident X-ray beam. It can be achieved systematically, according to Renninger (1937), by first placing the crystal so as to have a two-beam reflection, the so-called primary reflection, and then by rotating the crystal around the reciprocal-lattice vector of the primary reflection to bring other reciprocal-lattice points onto the Ewald sphere, thus obtaining the secondary reflections. Fig. 1 shows the geometry in reciprocal space. **P** and **H** are the reciprocal-lattice vectors for the primary and secondary reflections. $\mathbf{H}_n$ and $\mathbf{H}_p$ are the components of **H** normal and parallel to **P**. The radius of the Ewald sphere is $1/\lambda$, where λ is the wavelength of the X-rays used. Following Cole *et al.* (1962), the angle β, between $\mathbf{H}_n$ and the plane of incidence, p, of the primary reflection is given as

$$\cos\beta = [H^2 - H_p P]/[2H_n(1/\lambda^2 - P^2/4)^{1/2}]. \quad (1)$$

The azimuthal rotation angles φ around **P** from a reference vector, **V**, initially lying in the plane of incidence p, perpendicular to **P**, are $\chi - \beta$ and $\chi + \beta$ for the in-coming and out-going positions, respectively. χ is the angle between **V** and $\mathbf{H}_n$. For [001] InGaAsP compound layers (1) can be written as

$$\cos\beta = \left[\frac{h^2+k^2}{a_\parallel^2} + \frac{(l^2 - l - L)}{a_\perp^2}\right]\left[2\frac{(h^2+k^2)}{a_\parallel^2}\right]^{-1} \times \left[\frac{1}{\lambda^2} - \frac{L^2}{4a_\perp^2}\right]^{-1} \quad (2)$$

if the primary reflection is 001 and the secondary reflection hkl. Let us call β_0 the angle for a given multiple diffraction from the InP substrate. For small variations of $\Delta a_\perp$ and $\Delta a_\parallel$, in the quaternary materials, the deviation, $\Delta\beta$, from β_0 can be determined as

$$\Delta\beta = [(h^2+k^2)\Delta a_\parallel + (l^2 - lL)\Delta a_\perp] \times a_s[h^2+k^2]^{-1/2}[1/\lambda - L^2/4a_s^2]^{-1}. \quad (3)$$

This means that for nonzero $\Delta\beta$ a higher-order multiple simultaneous diffraction from a cubic lattice can be decomposed into a number of lower-order reflections of a tetragonal lattice. For instance, a six-beam case may be decomposed into two four-beam cases. We will now consider the following three interesting cases:

(*A*) *Five-beam*, 000, 006, $3\bar{3}3$, $\bar{1}11$, $\bar{1}15$, *case*

The five-beam simultaneous Bragg diffraction of InP in reciprocal space is shown in Fig. 2. As $a_\parallel$ and $a_\perp$ vary, the five reciprocal-lattice points can no longer be brought onto the Ewald sphere simultaneously during the rotation about [006]. The five-beam case is decomposed into three-beam, 000, 006, $3\bar{3}3$, and

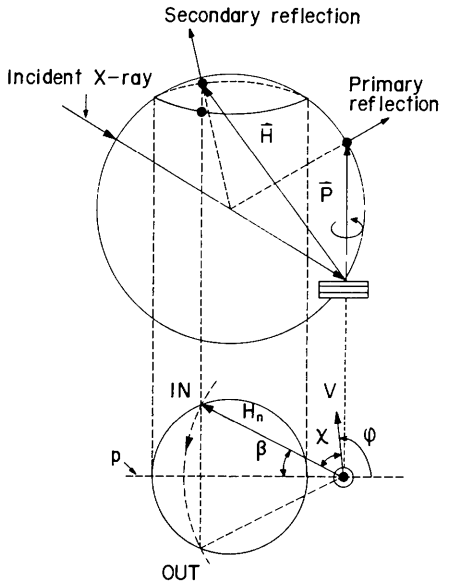

Fig. 1. Geometry of multiple diffraction in reciprocal space. The lower figure is a projection of the upper one on the plane perpendicular to the plane of incidence, p, of the primary reflection.

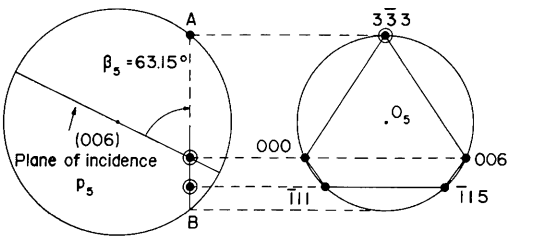

Fig. 2. Projections of the five-beam case on the plane perpendicular to the plane of incidence p_5 of 006 and on the plane containing the five reciprocal-lattice points.

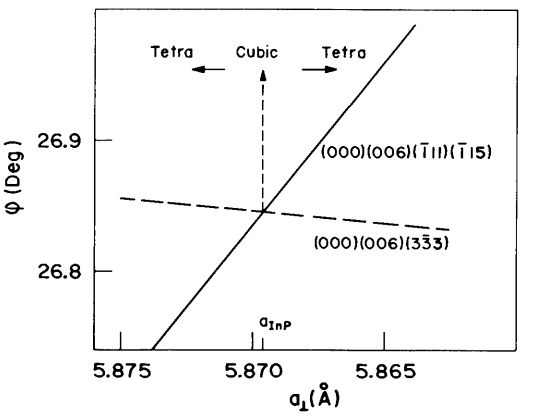

Fig. 3. Calculated azimuthal angles φ *vs* $a_\perp$ in the vicinity of the five-beam diffracting point for $a_\perp = a_{InP}$ and Cu $K\alpha_1$ radiation, with [1$\bar{1}$0] as the reference vector. At $a_\perp = a_{InP}$ the crystal is cubic. Otherwise, it is tetragonal. a_{InP} is the lattice constant for InP.

four-beam, 000, 006, $\bar{1}11$, $\bar{1}15$, simultaneous reflections. Since the $3\bar{3}3$ reciprocal-lattice point lies on one side while $\bar{1}11$ and $\bar{1}15$ lie on the other side of the [006] rotation axis, the relative motion of the reciprocal-lattice points of the four-beam case with respect to the Ewald sphere has an opposite sense to that of the three-beam case. During the rotation about [006], because of these relative motions the four-beam case enters just after the three-beam case leaves the Ewald sphere. The calculated azimuthal positions relative to the reference vector [1$\bar{1}$0] are given in Fig. 3. The inclination of the lines for the four-beam case is more pronounced than that for the three-beam case. For $a_\perp > a_s$, the ordering of the sequence of the points traversing the Ewald sphere is reversed: the three-beam enters just after the four-beam leaves the Ewald sphere. The cross point indicates the azimuthal position of the five-beam case for the InP substrate.

(*B*) *Eight-beam*, 000, 006, 020, 026, 0$\bar{2}$2, 0$\bar{2}$4, 042, 044, *case*

The eight-beam reflection of InP, shown in Fig. 4, is decomposed into three four-beam reflections for InGaAsP. They are, in the ordering of traversing the Ewald sphere, 000, 006, 0$\bar{2}$2, 0$\bar{2}$4; 000, 006, 020, 026; and 000, 006, 042, 044 for $a_\perp < a_s$. The last four-beam case enters after the other two cases leave the Ewald sphere. For $a_\perp > a_s$, the ordering is reversed. The calculated azimuthal φ are given as functions of $a_\perp$ in Fig. 5, where $a_\parallel$ was assumed to be unchanged.

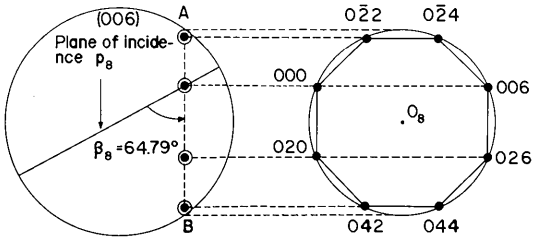

Fig. 4. Projections of the eight-beam case on the plane perpendicular to the plane of incidence, p_8, of 006 and on the plane containing the eight reciprocal-lattice points.

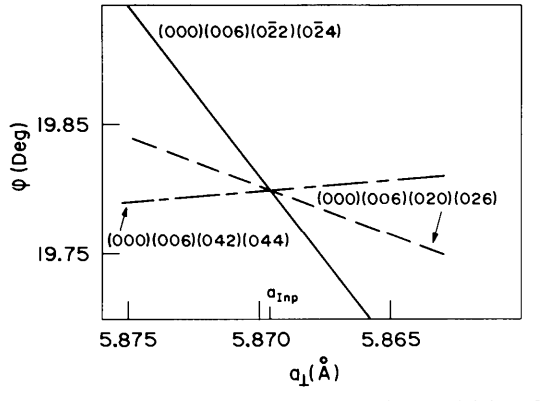

Fig. 5. Calculated azimuthal angles φ *vs* $a_\perp$ in the vicinity of the eight-beam diffracting point for $a_\parallel = a_{InP}$ and Cu $K\alpha_1$ radiation, with [1$\bar{1}$0] as the reference vector.

Intensity

For simplicity, we consider here a general four-beam simultaneous reflection from a double heterojunction plate, shown in Fig. 8. l_1, l_2 and m_1, m_2 are two transmitted (Laue) and two Bragg reflections, respectively. The incident beam is l_1. The heterojunction is composed of two InP layers, a cladding (S_1) and substrate (S_2), and a quaternary epi-layer Q in between. The thicknesses for S_1, S_2 and Q layers are d_1, d_2 and d_0. The Q layer is assumed to have a large lattice mismatch to the substrate such that multiple diffraction cannot take place simultaneously for both

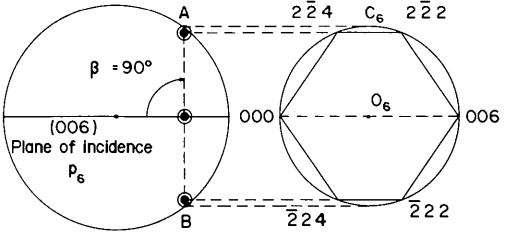

Fig. 6. Projections of the six-beam case on the plane perpendicular to the plane of incidence of 006 and on the plane containing the six reciprocal-lattice points.

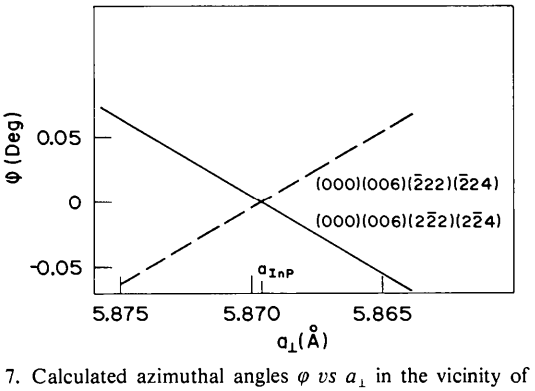

Fig. 7. Calculated azimuthal angles φ *vs* $a_\perp$ in the vicinity of the six-beam diffracting point for $a_\parallel = a_{InP}$ and Cu $K\alpha_1$ radiation, with [1$\bar{1}$0] as the reference vector.

InP and the quaternary layer at a given wavelength. When the layers S_1 and S_2 are in position to diffract an incident X-ray beam, an infinite number of reflections and transmissions take place. As illustrated in Figs. 9 and 10, the diffraction process involves the following successive steps. (1) Diffraction of the incident beam l_1 by layer S_1 (Fig. 9*a*): beam l_1 with an incident power $P_{l_1}(0)$ (assuming it is equal to unity at the entrance surface, $x = 0$) generates, at $x = d_1$, two transmitted beams, l_1 and l_2, with powers equal to $P_{l_1}(d_1)$ and $P_{l_2}(d_1)$; and, at $x = 0$, two zeroth-order reflected beams, m_1 and m_2, with reflection powers $P^0_{m_1}(0)$ and $P^0_{m_2}(0)$. $\mathbf{R}_{l_1}(d_1)$ and $\mathbf{T}_{l_1}(d_1)$ are the reflection and transmission operators which will be determined later. (2) Absorption of the two transmitted beams, l_1 and l_2, by the Q layer: the transmitted powers $P_{l_1}(d_1)$ and $P_{l_2}(d_1)$ suffer ordinary absorption through the operator $U_l(d_0)$ when traversing the Q layer. (3) Diffractions of l_1 and l_2 beams by layer S_2 (Figs. 9*b* and *c*): in this step, multiple diffraction takes place for each of the incident l_1 and l_2 beams. They generate two sets of reflected and transmitted beams through the operators $R_{l_1}(d_2)$, $T_{l_1}(d_2)$ and $R_{l_2}(d_2)$, $T_{l_2}(d_2)$. For l_1 beam, the total zeroth-order transmitted power, $P^0_{l_1}(d_1 + d_0 + d_2)$, emerging from the lower surface of S_2 ($x = d_1 + d_0 + d_2$), is the sum of the transmitted powers in the direction l_1, generated by both incident l_1 and l_2 beams. It is similar for the l_2 beam. For the reflected m_1 and m_2, the total powers at the upper surface of S_2 ($x = d_0 + d_1$) are $P_{m_1}(d_1 + d_0)$ and $P_{m_2}(d_1 + d_0)$, which remain to participate in the next diffraction step. (4) Absorption of the two reflected beams m_1 and m_2 by the Q layer: the corresponding reflection powers, $P_{m_1}(d_1 + d_0)$ and $P_{m_2}(d_1 + d_0)$, suffer absorption through the operator $U_m(d_0)$ when beams m_1 and m_2 traverse the Q layer. (5) Backward diffractions of reflected beams from layer S_1 (Figs. 9*d* and *e*): this step is similar to step (3) except that beams m_1 and m_2 are now transmitted beams while l_1 and l_2 are the reflected ones. The first-order reflected powers, $P^1_{m_1}(0)$ and $P^1_{m_2}(0)$, at $x = 0$, and the transmitted $P_{l_1}(d_1)$ and $P_{l_2}(d_1)$ at $x = d_1$, are generated by the transmission and reflection operators, $X_{m_1}(d_1)$, $X_{m_2}(d_1)$ and $D_{m_1}(d_1)$, $D_{m_2}(d_1)$, respectively. The repetition of steps (2), (3), (4) and (5) then follow to complete the diffraction process (Fig. 10). Since the steps (3) and (5) are similar to step (1) and the steps (2) and (4) are merely the attenuation of diffracted beams by the Q layer, in the following we first look for the formulation for the operators T and R for step (1) and then generalize it for steps (3) and (5).

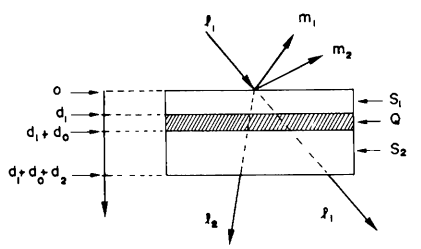

Fig. 8. Schematic representations of multiple diffraction from a sample containing InP layers, S_1 and S_2, and a quaternary layer, Q. l_1 and l_2 are the transmitted beams. m_1 and m_2 are the reflected ones.

Following Moon & Shull (1964), the differential equation describing the change in power in various beams as they traverse a crystal layer of thickness dx at depth x below the upper surface of layer S_1 can be written as

$$\pm \frac{\mathrm{d}P_i}{\mathrm{d}x} = -\frac{P_i}{\gamma_i}\mu + \sum_j \left(\frac{Q_{ji}P_j}{\gamma_j} - \frac{Q_{ij}P_i}{\gamma_i} \right), \qquad (4)$$

where the positive sign is for transmission and the negative one for reflection. P_i is the power in beam i, γ_i

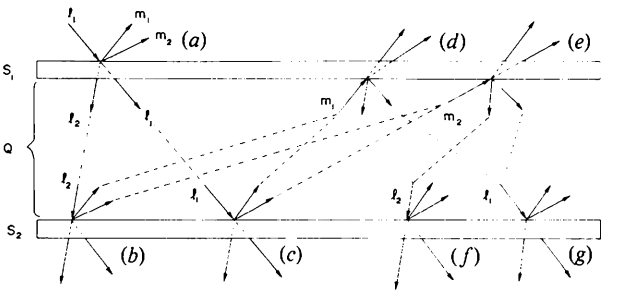

Fig. 9. Multiple diffractions from a double-layer system. Except for (*a*), only the incident beams are labeled in (*b*), (*c*), (*d*), (*e*), (*f*) and (*g*).

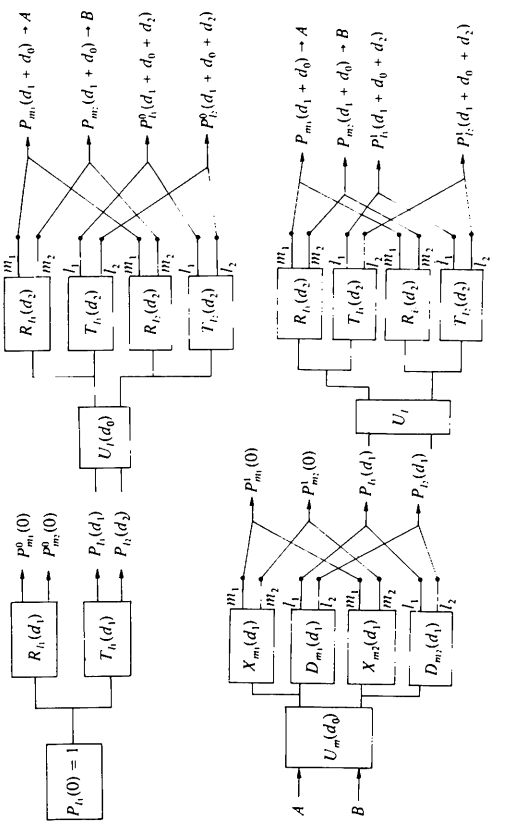

Fig. 10. Block diagram of multiple diffractions from a double-layer system.

is the magnitude of the direction cosine of beam i relative to the crystal surface normal and μ is the linear absorption coefficient. Q_{ij}, the effective reflectivity of reflection from planes $(i–j)$, is defined as

$$Q_{ij}=\left(\frac{\lambda^3 N_0^2|F_s|^2}{\sin 2\theta}\right)_{ij} W(\Delta\theta_{ij}), \tag{5}$$

where $W(\Delta\theta_{ij})$ is the mosaic distribution function of $\Delta\theta_{ij}$, the deviation from the Bragg angle of $(i-j)$ reflection. N_0 is the number of unit cells per unit volume, and F_s is the structure factor. An approximate solution of (1) for the power at $x = d_1$ can be assumed to be a Taylor series expansion about $x = 0$, *i.e.*

$$P_i(d_1)=\sum_{n=0}^{\infty}\frac{d_1^n}{n!}P_i^{(n)}(0) \tag{6}$$

for $i = l_1, l_2, m_1$ and m_2, where $P_i^{(n)}(0)$ is the nth-order derivative with respect to x at $x = 0$, and $P_i^{(0)}(0) = P_i(0)$. For X-ray diffraction in highly absorbing materials with respect to the radiation used, the condition, $\mu L_i \ll 1$ (where the path length $L_i = d_1/\gamma_i$), for the validity of Taylor series expansion is usually not fulfilled. It is, however, possible to have a convergent Taylor series, with its value very close to the exact solution, by including high-order terms. Since derivatives are also a function of the powers of all reflections, the nth-order term can be written as (Parente & Caticha-Ellis, 1974)

$$P_i^{(n)}(x)=\sum_{j_1}\sum_{j_2}\cdots\sum_{j_n} Y_{ij_1}Y_{j_1j_2}Y_{j_2j_3}\cdots Y_{j_{n-1}j_n}P_{j_n}(x), \tag{7}$$

where the j's can be l_1, l_2, m_1 and m_2, and

$$\begin{aligned} Y_{j_pj_q}&=S_{j_q}Q_{j_pj_q}/\gamma_{j_q} \quad \text{for } j_p\neq j_q,\\ Y_{j_pj_p}&=-S_{j_p}A_{j_p}/\gamma_{j_p} \quad \text{for } j_p=j_q \end{aligned} \tag{8}$$

with

$$A_{j_p}=\mu+\sum_{j_r\neq j_p} Q_{j_pj_r} \tag{9}$$

and

$$S_{j_p}=\begin{cases} + & \text{for transmitted beam}\\ - & \text{for reflected beam.}\end{cases}$$

For simplicity, define

$$a_{i,j_n}(d_1)=\sum_{n=0}^{\infty}\frac{d_1^n}{n!}\sum_{j_1}\sum_{j_2}\cdots\sum_{j_{n-1}} Y_{ij_1}Y_{j_1j_2}\cdots Y_{j_{n-1}j_n}. \tag{10}$$

By combining (6), (7) and (10), (6) has the following simple form:

$$P_i(d_1)=\sum_j a_{i,j}(d_1)P_j(0), \tag{11}$$

where the sum is taken over all reflections involved in the process. With the boundary conditions at the upper and lower surfaces of layer S_1, *i.e.*

$$P_{l_1}(0)=1,\quad P_{l_2}(0)=0,\quad P_{m_1}(d_1)=0 \quad \text{and}$$
$$P_{m_2}(d_1)=0,$$

the approximate solution of (4) can be obtained as

$$\begin{bmatrix} P_{l_1}(d_1)\\ P_{l_2}(d_2)\\ P_{m_1}(0)\\ P_{m_2}(0)\end{bmatrix}=\mathbf{B}_{l_1}(d_1)P_{l_1}(0), \tag{12}$$

where the vector

$$\mathbf{B}_{l_1}(d_1)=\mathbf{S}_{l_1}^{-1}(d_1)\mathbf{V}_{l_1}(d_1) \tag{13}$$

with

$$\mathbf{S}_{l_1}(d_1)=\begin{bmatrix} 1 & 0 & -a_{l_1m_1}(d_1)-a_{l_1m_2}(d_1)\\ 0 & 1 & -a_{l_2m_1}(d_1)-a_{l_2m_2}(d_1)\\ 0 & 0 & -a_{m_1m_1}(d_1)-a_{m_1m_2}(d_1)\\ 0 & 0 & -a_{m_2m_1}(d_1)-a_{m_2m_2}(d_1)\end{bmatrix}$$

and

$$\mathbf{V}_{l_1}(d_1)=\begin{bmatrix} a_{l_1l_1}(d_1)\\ a_{l_2l_1}(d_1)\\ a_{m_1l_1}(d_1)\\ a_{m_2l_1}(d_1)\end{bmatrix}.$$

The subscript l_1 in $\mathbf{B}_{l_1}$, $\mathbf{V}_{l_1}$ and $\mathbf{S}_{l_1}$ indicates that the incident beam is l_1. Since multiple diffraction involves transmission and reflection, it would be convenient to decompose (12) into two parts, one for transmission and the other for reflection:

$$\mathbf{P}_L(d_1)=\begin{bmatrix} P_{l_1}(d_1)\\ P_{l_2}(d_1)\end{bmatrix}=\mathbf{T}_{l_1}(d_1)P_{l_1}(0) \tag{14}$$

and

$$\mathbf{P}_M^0(0)=\begin{bmatrix} P_{m_1}^0(0)\\ P_{m_2}^0(0)\end{bmatrix}=\mathbf{R}_{l_1}(d_1)P_{l_1}(0), \tag{15}$$

where

$$\mathbf{T}_{l_1}(d_1)=\begin{bmatrix} b_{l_1l_1}(d_1)\\ b_{l_2l_1}(d_1)\end{bmatrix},\quad \mathbf{R}_{l_1}(d_1)=\begin{bmatrix} b_{m_1l_1}(d_1)\\ b_{m_2l_1}(d_1)\end{bmatrix}. \tag{16}$$

The elements, the b's, can be obtained from (13). The superscript 0 of P_M^0, $P_{m_1}^0$ and $P_{m_2}^0$ means the zeroth order of reflection from the upper surface of layer S_1. Hereafter, small letters with subscripts indicate the

elements of the corresponding vectors or matrices labeled with their capital letters.

Similarly, $T_{l_2}(d_2)$ and $R_{l_2}(d_2)$ can be obtained by just substituting l_1 and d_1 by l_2 and d_2 in the above expressions. For determining $\mathbf{X}_{m_1}(d_1)$ and $\mathbf{D}_{m_1}(d_1)$, (13) is replaced by

$$\mathbf{C}_{m_1}(d_1) = \mathbf{S}_{m_1}^{-1}(d_1)\,\mathbf{V}_{m_1}(d_1), \tag{17}$$

where $V_{m_1}(d_1)$ is equivalent to $V_{l_1}(d_1)$ except for changing l_1 to m_1, and $\mathbf{S}_{m_1}(d_1)$ is defined as

$$\mathbf{S}_{m_1}(d_1) = \begin{bmatrix} -a_{l_1\,l_1}(d_1) & -a_{l_1\,l_2}(d_1) & 0 & 0 \\ -a_{l_2\,l_1}(d_1) & -a_{l_2\,l_2}(d_1) & 0 & 0 \\ -a_{m_1\,l_1}(d_1) & -a_{m_1\,l_2}(d_1) & 1 & 0 \\ -a_{m_2\,l_1}(d_1) & -a_{m_2\,l_2}(d_1) & 0 & 1 \end{bmatrix}.$$

The operators $\mathbf{X}_{m_1}(d_1)$ and $\mathbf{D}_{m_1}(d_1)$ are then obtained as

$$\mathbf{X}_{m_1}(d_1) = \begin{bmatrix} C_{m_1\,m_1}(d_1) \\ C_{m_2\,m_1}(d_1) \end{bmatrix}$$

and

$$\mathbf{D}_{m_1}(d_1) = \begin{bmatrix} C_{l_1\,m_1}(d_1) \\ C_{l_2\,m_1}(d_1) \end{bmatrix} \tag{18}$$

and similarly for $\mathbf{X}_{m_2}(d_1)$ and $\mathbf{D}_{m_2}(d_1)$. By considering the ordinary absorption, the operators $U_l(d_0)$ and $U_m(d_0)$ have the following simple form:

$$U_l(d_0) = \begin{bmatrix} u_{l_1}(d_0) \\ u_{l_2}(d_0) \end{bmatrix}$$

and

$$U_m(d_0) = \begin{bmatrix} u_{m_1}(d_0) \\ u_{m_2}(d_0) \end{bmatrix}, \tag{19}$$

where $u_l(d_0) = \exp(-\mu_0 d_0/\gamma_l)$, μ_0 being the linear absorption coefficient for the Q layer with respect to the radiation used.

With the aid of Fig. 10 the reflected powers of m_1 and m_2 from the upper surface of layer S_1 are obtained for various orders of reflection from (16), (18) and (19) as

$$\mathbf{P}_M^0(0) = \mathbf{R}_{l_1}(d_1)\,P_{l_1}(0)$$

$$\mathbf{P}_M^1(0) = \mathbf{X}(d_1)\,\mathbf{R}_u(d_2)\,\mathbf{T}_u(d_1)\,P_{l_1}(0)$$

$$\mathbf{P}_M^2(0) = \mathbf{X}(d_1)[\mathbf{R}_u(d_2)\,\mathbf{D}_u(d_1)]\,\mathbf{R}_u(d_1)\,\mathbf{T}_u(d_1)\,P_{l_1}(0)$$

$$\mathbf{P}_M^3(0) = \mathbf{X}(d_1)[\mathbf{R}_u(d_2)\,\mathbf{D}_u(d_1)]^2\,\mathbf{R}_u(d_1)\,\mathbf{T}_u(d_1)\,P_{l_1}(0)$$

and

$$\mathbf{P}_M^n(0) = \mathbf{X}(d_1)[\mathbf{R}_u(d_2)\,\mathbf{D}_u(d_1)]^{n-1}\,\mathbf{R}_u(d_1)\,\mathbf{T}_u(d_1)\,P_{l_1}(0) \tag{20}$$

for the nth-order reflection, where

$$\mathbf{X}(d_1) = [\mathbf{X}_{m_1}(d_1),\, \mathbf{X}_{m_2}(d_1)]$$

$$\mathbf{R}_u(d_2) = \begin{bmatrix} u_{m_1}(d_0)\,r_{m_1\,l_1}(d_2) & u_{m_1}(d_0)\,r_{m_1\,l_2}(d_2) \\ u_{m_2}(d_0)\,r_{m_2\,l_1}(d_2) & u_{m_2}(d_0)\,r_{m_2\,l_2}(d_2) \end{bmatrix}$$

$$\mathbf{D}_u(d_2) = \begin{bmatrix} u_{l_1}(d_0)\,d_{l_1\,m_1}(d_1) & u_{l_1}(d_0)\,d_{l_1\,m_1}(d_1) \\ u_{l_2}(d_0)\,d_{l_2\,m_2}(d_1) & u_{l_2}(d_0)\,d_{l_2\,m_2}(d_1) \end{bmatrix}$$

$$\mathbf{T}_u(d_1) = u_{l_1}(d_0)\begin{bmatrix} t_{l_1\,l_1}(d_1) \\ t_{l_2\,l_1}(d_1) \end{bmatrix}$$

and $P_{l_1}(0) = 1$. The total reflected power is then

$$\mathbf{P}_M^T(0) = \sum_{n=0}^{\infty} \mathbf{P}_M^n(0)$$

$$= \mathbf{R}_l(d_1) + \mathbf{X}(d_1)[\mathbf{I}_M - \mathbf{F}(d_2,d_1)]^{-1}\,\mathbf{G}(d_2,d_1), \tag{21}$$

where $[\mathbf{I}_M - \mathbf{F}]^{-1}$ is the inverse matrix of $\mathbf{I}_M - \mathbf{F}$, $\mathbf{I}_M$ is the unit matrix, and $\mathbf{F}$ and $\mathbf{G}$ are defined as $\mathbf{F}(d_2,d_1) = \mathbf{R}_u(d_2)\,\mathbf{D}_u(d_1)$ and $\mathbf{G}(d_2,d_1) = \mathbf{R}_u(d_2)\,\mathbf{T}_u(d_1)$. All the elements of $\mathbf{F}$ are much less than 1 for X-ray cases.

Similarly, the transmitted powers of the nth order, emerging from the lower surface of layer S_2, have the following form:

$$\mathbf{P}_L^n(d_1 + d_0 + d_2) = \mathbf{T}(d_2)[\mathbf{D}_u(d_1)\,\mathbf{R}_u(d_2)]^n\,\mathbf{T}_u(d_1), \tag{22}$$

where $\mathbf{T}(d_2) = [\mathbf{T}_{l_1}(d_2),\, \mathbf{T}_{l_2}(d_2)]$. The total transmitted powers are

$$\mathbf{P}_L^T(d_1 + d_0 + d_2) = \sum_{n=0}^{\infty} \mathbf{P}_L^n(d_1 + d_0 + d_2)$$

$$= \mathbf{T}(d_2)[\mathbf{I}_L - \mathbf{E}(d_1,d_2)]^{-1} \times \mathbf{T}_u(d_1), \tag{23}$$

where $\mathbf{E}(d_1,d_2) = \mathbf{D}_u(d_1)\,\mathbf{R}_u(d_2)$ and $\det|\mathbf{E}| \ll 1$ for X-ray cases.

The above treatment is for multiple diffraction from a double-layer system, for example the DH sample with a lattice-mismatched Q layer. If the Q layer has the same lattice constant as the S_1 and S_2 layers, diffractions from a triple-layer system should be considered. This treatment is given in the Appendix. For simple SH samples, the treatment for double layers can be used by setting d_1 equal to zero. Moreover, it is applicable to cases involving only a single crystal plate by assuming $d_1 = d_2 = 0$ and d_0 equal to the thickness of the plate.

Equations (21) and (23) can be generalized for any n-beam simultaneous reflection, in which n_T transmissions and n_R reflections are involved. The corresponding dimensions of vectors $\mathbf{R}_{l_1}$, $\mathbf{G}$ and $\mathbf{T}_u$ are $(n_R \times 1)$, $(n_R \times 1)$, and $(n_T \times 1)$, and of matrices $\mathbf{X}$, $\mathbf{R}_u$, $\mathbf{D}_u$, $\mathbf{T}$, $\mathbf{I}_L$, $\mathbf{I}_M$, $\mathbf{F}$ and $\mathbf{E}$ are $(n_R \times n_R)$, $(n_R \times n_T)$,

$(n_T \times n_T)$, $(n_T \times n_T)$, $(n_T \times n_T)$, $(n_R \times n_R)$, $(n_R \times n_R)$ and $(n_T \times n_T)$, respectively. A computer program for calculating the peak intensities of a general n-beam case was written based on the above treatment with the mosaic distribution $\bar{W} = 1$, assuming that the mosaic spreads of the samples are the same.

There are a few remarks about the computing procedure which need to be mentioned.

(1) *Calculation for high-order derivatives and the polarization factors*

An iterative way of calculating a high-order derivative from the next high-order one was originally derived for multiple diffraction of neutrons (Parente & Caticha-Ellis, 1974). For neutron diffraction, the fact that polarization need not be considered facilitates the iterative calculation. It is, however, difficult in X-ray cases to put correct polarization factors in the iterative method. The reason is that the polarization factor in Y_{ij} of (7) depends not only on the $(i–j)$ reflection but on the ordering in the sequence of the successive reflections, *i.e.* $i–j_1$, $j_1–j_2$, $j_2–j_3$,... (Zachariasen, 1965; Caticha-Ellis, 1969; Unangst & Melle, 1975). Hence, for each iterative cycle, a new polarization factor has to be put in the calculation since one more reflection is being added to the sequence of reflections. This is not only inconvenient but it is impossible for the program to handle correctly and simultaneously the polarization factors and the iteration. In order to overcome this difficulty, a test has been carried out with two different expressions for polarization factors; one is $P_{ij} = (1 + \cos^2 2\theta_{ij})/2$ for a simple two-beam reflection $i–j$, the other is, from Zachariasen (1965),

$$P_{ij}(i–j) = \tfrac{1}{2}[\cos^2 2\theta_i + \cos^2 2\theta_j + (\cos 2\theta_{i-j} - \cos 2\theta_i \cos 2\theta_j)^2] \quad (24)$$

considering the sequence of first two successive reflections involved in a given multiple diffraction. It turned out that both gave almost the same 006 reflected intensities. Equation (24) was therefore used throughout the calculations.

(2) *Multiple diffraction involving surface reflection*

The five-beam case involves a surface reflection 333, whose diffracted wavevector is along the crystal surface. The direction cosine γ_{333} gives an infinite path length. However, as the surface reflection is a case between Laue transmission and Bragg reflection, 333 can be treated either as a Laue or as a Bragg reflection with a given γ_{333} very close to zero in calculation.

(3) *Temperature and anomalous scattering corrections*

The Debye parameters, $B_{\text{In}} = 0{\cdot}624$, $B_{\text{P}} = 0{\cdot}591$ (Post, 1975*a*) and $B_{\text{GaAs}} = 0{\cdot}60$ Å^2 (*International Tables for X-ray Crystallography*, 1968) were used for temperature correction on structure factors at room temperature. The corrections due to anomalous scattering were also included.

Experimental

(i) *Divergent-beam experiment*

The divergent-beam experimental set-up described by Chang *et al.* (1979) was employed. The schematic representation is shown in Fig. 11. The 5° divergence facilitates the crystal alignment and permits the recording in one photograph of regions in reciprocal space included within a 5° azimuthal rotation. Films served as a detector for the 006 reflection. A Cu target was used.

The samples consisted of an InP single crystal and six InGaAsP/InP heterojunction plates, with their large faces, having areas about 5 × 5 mm, cut normal to [001]. The thicknesses of the InP substrate and the InGaAsP epitaxial layers were about 530 and 5 μm, respectively. These six heterojunction samples had a common value, 0·007, for X^I_{Ga} and 0·0105, 0·0099, 0·0091, 0·0083, 0·0077, 0·0064 for X^I_{As}, respectively.

The experiment was performed by first setting the sample in position for the 006 reflection and then by rotating the sample around [006] to the pre-calculated azimuthal φ positions, *i.e.* 26·85, 0·0 and 19·79° for the above mentioned five-, six- and eight-beam reflections, respectively, $[1\bar{1}0]$ being the reference vector. The exposure time for Kodak XRP films was 45 min when the Rigaku microfocus X-ray generator was operated at 40 kV, 0·3 A filament current and 0·5 mA beam current.

(ii) *Collimated-beam experiment*

The experimental set-up, similar to that reported by Renninger (1937), consisted of (1) a collimator which permitted the angular divergence of an incident beam to about 20′ of arc, (2) a Philips goniostat adapted with a

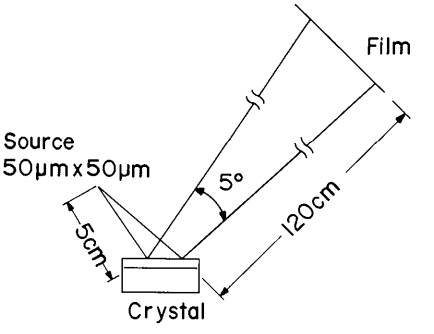

Fig. 11. Schematic representation of the divergent-beam experimental set-up.

Rigaku four-circle goniometer head, (3) a Spex driving system used to rotate a crystal around its surface normal, and (4) a scintillation counter. The distance between the Cu target and the sample was 200 mm. In all, an InP crystal, two SH samples, 20 and 55, and two DH samples, 22 and 84, were investigated. The thicknesses for the quaternary epilayers, InP cladding layers and substrate are listed in Table 1. The Ga and As concentrations, x and y, in solid composition at the quaternary compound layers, the corresponding lattice constants, and the linear absorption coefficients with respect to Cu $K\alpha_1$ and Cu $K\alpha_2$ are given in Table 2.

The sample was first aligned for 006 reflection. A θ–2θ scan (Fig. 12) was taken to locate the angular positions for 006 reflection peaks for Cu $K\alpha_1$ and Cu $K\alpha_2$ radiation from both the substrate and quaternary layers. The sample was then set at the corresponding Bragg angle, θ_B, for either the substrate or the quaternary layer, and rotated around [006]. As secondary reflections entered and left the Ewald sphere, the resultant interaction among reflections within the crystal gave rise to variations in the intensity of the primary, 006, reflection. Figs. 13, 14 and 15 show the 45° asymmetric portion of multiple diffraction patterns for the InP substrate and samples 20 and 22. Their Bragg angles were set at the positions having maximum intensities in the 006 θ–2θ scans for Cu $K\alpha_1$ and Cu $K\alpha_2$ radiation, shown in Fig. 12. Note that, for 20 and 22, the 006 reflection peaks from InP for Cu $K\alpha_2$ and from the quaternary layer for Cu $K\alpha_1$ overlap owing to beam divergence and the differences in lattice constant between the quaternary materials and InP. In Figs. 13, 14 and 15, only the five- and eight-beam cases have notable intensities above the 006 reflection background. The diffracted peak intensity for each of these two cases was measured for 100 s for the five samples with Cu $K\alpha_1$ and Cu $K\alpha_2$ radiation.

Table 1. *The thicknesses of layers, in* μm, *for the samples studied*

	Sample				
Layer	InP	20	55	22	84
InP–cladding d_1	0	0	0	2·0	2·0
Quaternary d_0	0	2·0	2·0	1·6	0·3
Substrate d_2	530·0	530·0	530·0	530·0	530·0

Results and discussion

(i) *Divergent-beam experiment*

Figs. 16(*a*) and (*b*) show the enlarged (×4) photographic images of the five-beam simultaneous diffraction for the InP substrate and of the three- and four-beam reflections for the InGaAsP/InP with X^I_{As} equal to 0·0083. The vertical lines are the 006 reflection lines from the substrate and epitaxial layer. It is known that $a_\perp$ varies continuously along the interface normal.

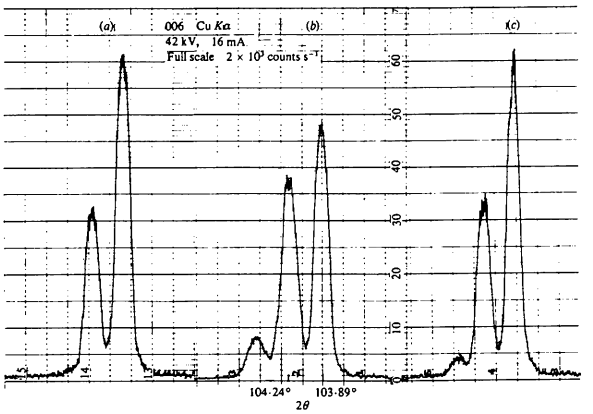

Fig. 12. θ–2θ scan of 006 reflections for Cu $K\alpha_1$ and Cu $K\alpha_2$ radiation from (*a*) an InP substrate, (*b*) sample 20 and (*c*) sample 22. In (*b*) and (*c*), the central peaks are the overlapped peaks of Cu $K\alpha_1$ from the quaternary layer.

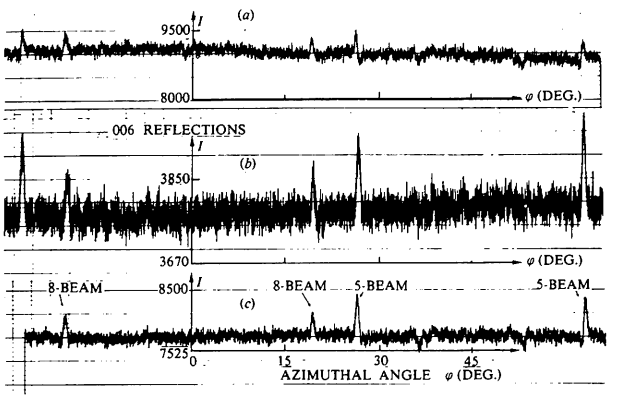

Fig. 13. 006 multiple diffraction patterns for Cu $K\alpha_1$ from InP layers for (*a*) an InP substrate, (*b*) sample 20 and (*c*) sample 22. Intensitv I in counts s^{-1}.

Table 2. *The solidus atomic concentrations, x and y, of gallium and arsenic in Q layers, their lattice constants a and linear absorption coefficients* μ

	Sample				
	InP	20	55	22	84
x	0	0·21	0·20	0·18	0·26
y	0	0·43	0·45	0·45	0·56
a (Å)	5·8696	5·8644	5·8723	5·8806	5·8696
μ(Cu $K\alpha_1$) (mm^{-1})	98·779	88·840	89·493	90·645	86·521
μ(Cu $K\alpha_1$) (mm^{-1})	99·568	89·357	90·031	91·191	87·035

A broad reflection band is common for the epi-layers. The cross-hatched pattern on the layer lines is a superposition of the surface morphology on the diffraction image. The directions parallel and perpendicular to the 006 reflection lines represent the angles φ and $\Delta\theta$. $\Delta\theta$ is the angular deviation from the Bragg angle θ_B of the 006 reflection. The image shown in Fig. 16(*b*) resembles the portion for $a_\perp < a_s$ in Fig. 3. The line for 000, 006, $3\bar{3}3$ is too weak to be seen. The effect of the variation in $a_\parallel$ on the diffraction image is so small that it cannot be detected by visual inspection. The inclination of the multiple diffraction lines with respect to the 006 line is because the β angles are not equal to zero. Given that the quaternary compound with $X^I_{As} = 0{\cdot}0083$ is less perfect than the InP substrate, as a single crystal is concerned, the intersection, shown in Fig. 16(*a*), between the diffraction lines of the 006 reflection and the four-beam reflection for InP is clearer than that shown in Fig. 16(*b*) for the quaternary layer.

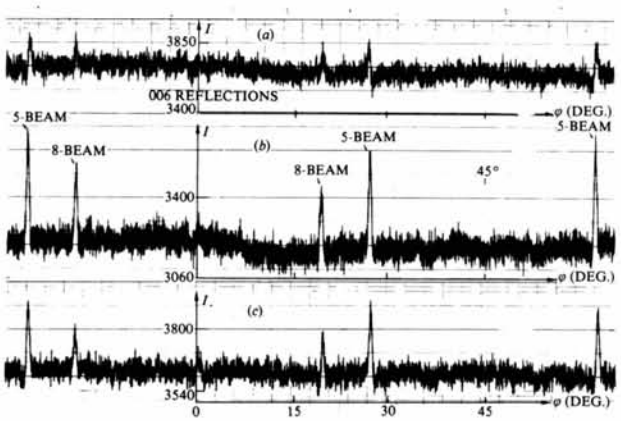

Fig. 14. Multiple diffraction patterns of (*a*) 006 reflection for Cu $K\alpha_2$ from InP substrate, (*b*) overlapped 006 reflection for Cu $K\alpha_2$ from the InP layer and Cu $K\alpha_1$ from the Q layer for sample 20 and (*c*) same as (*b*) but for sample 22.

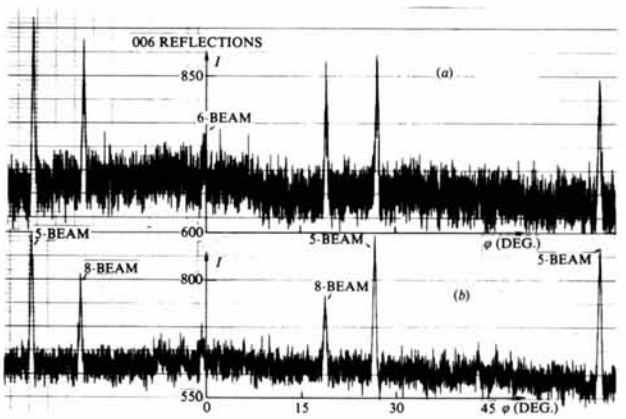

Fig. 15. 006 multiple diffraction patterns for Cu $K\alpha_2$ from the Q layer for (*a*) sample 20 and (*b*) sample 22. The peak at $\varphi = 0$ is due to the six-beam, 000, 006, $2\bar{2}2$, $2\bar{2}4$, $\bar{2}22$, $\bar{2}24$ case.

Figs. 16(*c*) and (*d*) are the diffraction images of the eight-beam case for the substrate and of the three four-beam cases for the epi-layer. According to Moon & Shull (1964), the diffracted intensities of these four-beam cases roughly depend on the square of the product of the structure factors of the secondary reflections and of their coupling reflections to 006. Since

$$|F_{0\bar{2}2}F_{0\bar{2}4}|^2 : |F_{020}F_{02\bar{6}}|^2 : |F_{044}F_{04\bar{2}}|^2 = 2{\cdot}5 : 1{\cdot}7 : 1{\cdot}0,$$

only the diffraction lines for 000, 006, $0\bar{2}2$, $0\bar{2}4$ and 000, 006, 020, 026 appeared.

Referring to (3), it would, in principle, be possible to draw the information for $\Delta a_\parallel$ and $\Delta a_\perp$ simultaneously from the line separation of the above mentioned four-beam reflections. By comparing Fig. 5 with Fig. 7, we see, however, that the line separation in Fig. 5 is smaller than that of Fig. 7 for a given $a_\perp$. The decomposition of the six-beam into two four-beam reflections might be more proper for the simultaneous determination of $\Delta a_\parallel$ and $\Delta a_\perp$. In Fig. 17, we show the images of the 006 reflection in the vicinities of the six-beam case for InP and the four-beam cases for InGaAsP for several values of X^I_{As}. The corresponding

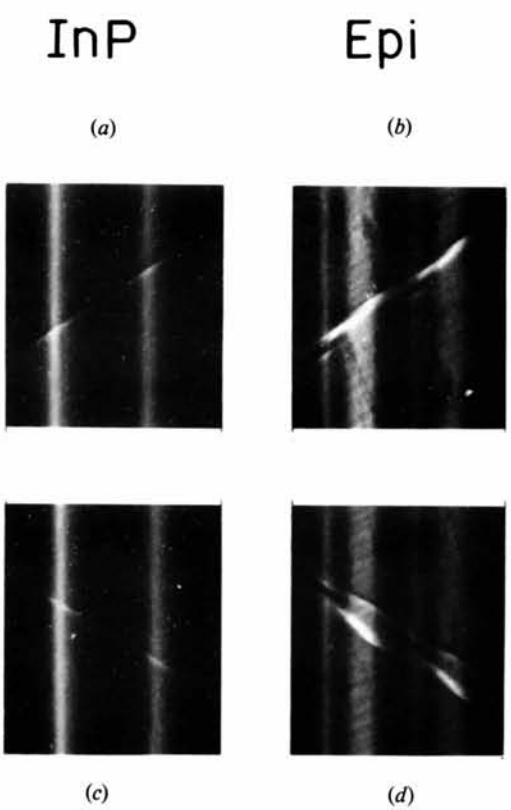

Fig. 16. The 006 reflection images in the vicinities of (*a*) the five-beam and (*c*) the eight-beam case for InP and of their corresponding (*b*) $\frac{3}{4}$-beam case and (*d*) four-beam cases for InGaAsP epi-layer with $X^I_{As} = 0{\cdot}0083$ and $X^I_{Ga} = 0{\cdot}0007$. Cu $K\alpha_1$ lines of (*b*) and (*d*) are on the left of Cu $K\alpha_2$ lines.

$\Delta a_{\parallel}$ and $\Delta a_{\perp}$ for each X^I_{As} can be obtained from the equation

$$\Delta\beta = 0{\cdot}25[\Delta a_{\parallel} - \Delta a_{\perp}] \qquad (25)$$

deduced from (3) for the six-beam case. $\Delta a_{\perp}$ and $\Delta\beta$ can be determined from $\Delta a_{\perp}/a_s = -\cot\theta_B \Delta\theta$ and from the angular separation between the two four-beam diffraction lines.

In Fig. 18, the measured $\Delta a_{\perp}$ and $\Delta a_{\parallel}$ are given as a function of X^I_{As} with $X^I_{Ga} = 0{\cdot}0007$. They resemble the curves obtained by Oe *et al.* (1978) for X^I_{As} and X^I_{Ga} one order of magnitude higher. The errors indicated here were estimated from the widths of the reflection lines.

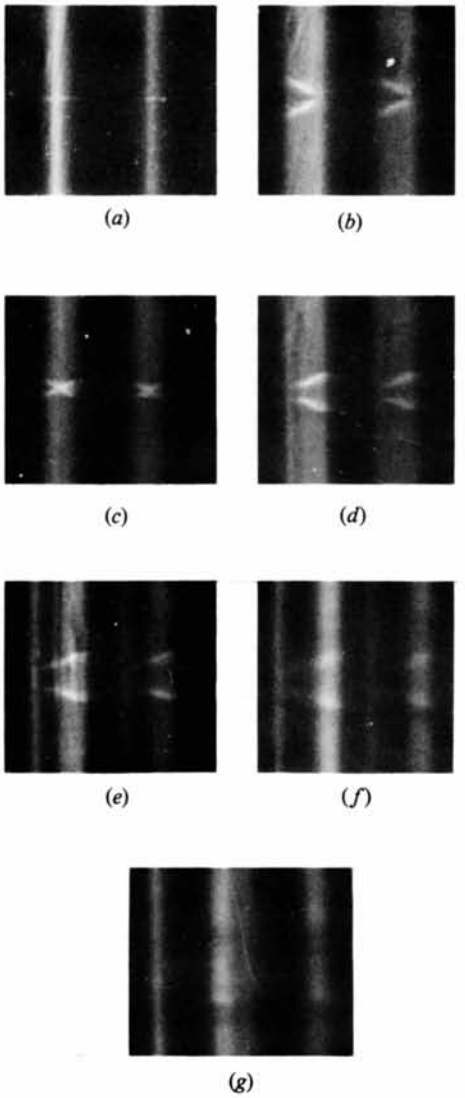

Fig. 17. The 006 reflection images in the vicinities of (*a*) the six-beam case for InP and of the four-beam case for InGaAsP with X^I_{As} equal to: (*b*) 0·0105, (*c*) 0·0099, (*d*) 0·0091, (*e*) 0·0083, (*f*) 0·0077 and (*g*) 0·0064, where $X^I_{Ga} = 0{\cdot}0007$. Cu $K\alpha_1$ lines are on the left of Cu $K\alpha_2$ lines.

(ii) *Collimated-beam experiment*

The observed and calculated intensities from the quaternary and InP layers are listed in Tables 3 and 4 for the eight-beam and five-beam cases, respectively. Comparison of the diffracted intensities from different samples can be made from I/I (22) columns, where the intensity diffracted from sample 22 was treated as unity. Better agreement between observed and calculated intensities can be seen in eight-beam cases than in five-beam cases. The choice of 10 μm ($\simeq 1/\mu$) for d_2 seems more appropriate for calculating diffracted intensities than the choice of the thicknesses such that

$$\sum_i \mu_i d_i = 1$$

where the summation is over all layers.

Comparison of the diffracted intensity of the eight-beam case, with that of the five-beam from the same sample can be made from Table 5. ΔI_8 and ΔI_5 are the differences in the 006 reflected intensity between two-beam 006 reflection and the five- and eight-beam cases, respectively. Tables 5(*A*) and 5(*B*) show qualitative agreements for I_5/I_8 and $\Delta I_8/\Delta I_5$ between the experimental and theoretical results. The agreement between the observed and calculated $\Delta I_8/\Delta I_5$ in Table 5(*C*) is rather poor owing to the relatively high background of weak reflections from the *Q* layers, and the uncertainty in their thicknesses. The former can also be seen from the diffraction patterns shown in Fig. 15. Relative standard deviations of $\Delta I_8/\Delta I_5$ average to about 15% for the values listed in Tables 5(*A*) and 5(*B*) and 100% for Table 5(*C*).

The main sources of errors are thought to be due to (*a*) variation of the surface conditions of the samples and (*b*) the absorption. As is known, the surface morphologies of LPE layers vary as their lattice

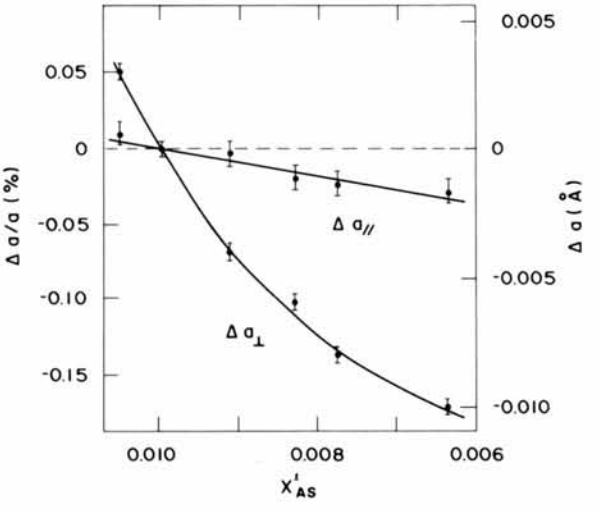

Fig. 18. Measured $\Delta a_{\parallel}$ and $\Delta a_{\perp}$ for various X^I_{As}, where $X^I_{Ga} = 0{\cdot}0007$.

Table 3. *Calculated (I_{calc}) and observed (I_{obs}) 006 reflected intensities for the eight-beam case*

Σ represents $\sum_i \mu_i d_i = 1$.

(*A*) Reflections from InP for Cu $K\alpha_1$ radiation

		I_{calc} (10^{-5})		I/I (22)		
Sample	I_{obs} (counts)	$d_2 = 10$ μm	Σ	Obs.	Calc. (10 μm)	Calc. (Σ)
InP	967 906	0·7185	0·7201	1·01	1·13	1·21
20	701 322	0·5036	0·4799	0·73	0·79	0·81
55	691 543	0·5023	0·4785	0·72	0·79	0·80
22	955 697	0·6341	0·5961	1·00	1·00	1·00
84	1 010 734	0·7346	0·7084	1·06	1·16	1·19

(*B*) Reflections from InP for Cu $K\alpha_2$ and from *Q* layers for Cu $K\alpha_1$

		I_{calc} (10^{-5})		I/I (22)		
Sample	I_{obs} (counts)	$d_2 = 10$ μm	Σ	Obs.	Calc. (10 μm)	Calc. (Σ)
InP	484 207	0·3905	0·3905	0·84	0·91	0·96
20	524 682	0·4175	0·4042	0·91	0·98	1·00
55	512 728	0·4144	0·4011	0·89	0·97	0·99
22	577 154	0·4263	0·4053	1·00	1·00	1·00
84	520 340	0·3991	0·3905	0·90	0·94	0·96

(*C*) Reflections from *Q* layers for Cu $K\alpha_2$

			I/I (22)	
Sample	I_{obs}	I_{calc} (10^{-6})	Obs.	Calc.
20	118 713	0·7860	1·59	1·76
55	101 425	0·7730	1·36	1·74
22	74 731	0·4454	1·00	1·00

Table 4. *Calculated (I_{calc}) and observed (I_{obs}) 006 reflected intensities for the five-beam case*

Σ represents $\sum_i \mu_i d_i = 1$.

(*A*) Reflections from InP for Cu $K\alpha_1$ radiation

		I_{calc} (10^{-5})		I/I (22)		
Sample	I_{obs} (counts)	$d_2 = 10$ μm	Σ	Obs.	Calc. (10μm)	Calc. (Σ)
InP	977 426	0·7190	0·7205	0·99	1·12	1·21
20	740 562	0·5457	0·4888	0·75	0·85	0·82
55	705 521	0·5442	0·4879	0·72	0·85	0·82
22	984 039	0·6391	0·5966	1·00	1·00	1·00
84	1 045 112	0·7410	0·7091	1·06	1·11	1·19

(*B*) Reflections from InP for Cu $K\alpha_2$ and from *Q* layers for Cu $K\alpha_1$

		I_{calc} (10^{-5})		I/I (22)		
Sample	I_{obs} (counts)	$d_2 = 10$ μm	Σ	Obs.	Calc. (10 μm)	Calc. (Σ)
InP	488 303	0·3908	0·3908	0·81	0·91	0·96
20	557 430	0·4417	0·4087	0·92	1·03	1·01
55	555 194	0·4385	0·4052	0·92	1·02	1·00
22	606 592	0·4293	0·4055	1·00	1·00	1·00
84	537 462	0·4086	0·3910	0·89	0·95	0·96

(*C*) Reflections from *Q* layers for Cu $K\alpha_2$

			I/I (22)	
Sample	I_{obs}	I_{calc} (10^{-6})	Obs.	Calc.
20	129 733	0·7870	1·50	1·77
55	108 349	0·7740	1·25	1·74
22	86 412	0·4458	1·00	1·00

Table 5. *Calculated and observed I_5/I_8 and $\Delta I_8/\Delta I_5$*

The thickness d_2 is 10 μm and Σ represents $\sum_l \mu_l d_l = 1$.

(*A*) Reflections from InP for Cu $K\alpha_1$

	I_5/I_8			$\Delta I_8/\Delta I_5$	
Sample	Obs.	Calc. (10 μm)	Calc. (Σ)	Obs.	Calc.
InP	1·01	1·00	1·00	0·70	0·71
20	1·06	1·08	1·02	0·75	0·71
55	1·02	1·08	1·02	0·61	0·71
22	1·03	1·01	1·00	0·63	0·70
84	1·03	1·01	1·00	0·60	0·69

(*B*) Reflections from InP for Cu $K\alpha_2$ and from *Q* layers for Cu $K\alpha_1$

	I_5/I_8			$\Delta I_8/\Delta I_5$	
Sample	Obs.	Calc. (10 μm)	Calc. (Σ)	Obs.	Calc.
InP	1·01	1·00	1·00	0·70	0·70
20	1·06	1·06	1·01	0·65	0·56
55	1·08	1·06	1·01	0·51	0·55
22	1·05	1·01	1·00	0·54	0·62
84	1·03	1·02	1·00	0·63	0·74

(*C*) Reflections from *Q* layers for Cu $K\alpha_2$

			$\Delta I_8/\Delta I_5$	
Sample	$(I_5/I_8)_{obs}$	$(I_5/I_8)_{calc}$	Obs.	Calc.
20	1·09	1·00	0·67	0·32
55	1·07	1·00	0·71	0·30
22	1·16	1·00	0·52	0·33

constants change. In principle, better surface morphologies are obtained in quaternary layers with less lattice mismatch to the substrate. According to Evans, Hirsch & Kellar (1948), the reflected intensities are affected a great deal by the conditions of the crystal surface. The influence of the surface conditions on the measured intensities in the present work is unavoidable since the surface conditions of the samples used are different from each other owing to the different lattice constants of the quaternary materials listed in Table 2. This can be observed from the variation of reflected background shown in Figs. 13, 14 and 15. Moreover, since the investigated five-beam cases involve a surface reflection, their reflected intensities were then affected by the surface conditions in degree greater than those for the eight-beam cases.

The other source of error is absorption. The theoretical treatment described above considered the absorption as the same for any *n*-beam case. That is, μ is always equal to the value of the normal linear absorption coefficient. As a matter of fact, the resultant interaction among the *n* diffracted beams may change the absorption. Usually, the resultant absorption coefficient in transmission cases is lower than the normal value. In order to take care of this fact, a dynamical theory of X-ray diffraction should be employed. This is beyond the scope of this paper. However, the investigation of dynamical diffraction aspects as applied to LPE multi-layer systems is in progress and will be reported later.

Conclusion

From the above photographic investigation, it is shown that although the concentration X^l_{Ga} is as low as 0·07% and X^l_{As} is less than 1%, the corresponding lattice mismatch between the InP substrate and InGaAsP layer affects enormously the images of simultaneous Bragg diffraction from this LPE heterojunction system. Consequently, the herein-described experiment provides a method of determining $\Delta a_{\parallel}$ and $\Delta a_{\perp}$ from a single divergent-beam X-ray photograph with multiple simultaneous Bragg diffraction. Clearly, this method is applicable to any [001] InGaAsP quaternary layer with high X^l_{Ga} and X^l_{As}. However, for [111]-oriented quaternary materials, one should look for other multiple diffraction sets for such investigations.

In the counter detection study, we have observed the effect of the concentrations, *x* and *y*, of the quaternary layer on the reflected intensities of simultaneous diffractions. This effect was qualitatively accounted for with the theory derived above. If the experimental conditions can be improved and the dynamical effects of diffraction can be taken into account, quantitative analysis on the concentrations, *x* and *y*, of epitaxial materials from the reflected intensities of simultaneous diffraction of X-rays could be possible.

The financial support from CNPq, BID and Telebrás is gratefully acknowledged.

APPENDIX

Diffracted powers of multiple diffraction from a triple-layer system

For simplicity, a sample, as shown in Fig. 19, is assumed to have two InP layers, S_1 and S_3, a quaternary layer S_2, and two absorbing layers, A_1 and A_2, of the same material. Their thicknesses are d_1, d_2 and d_3 for layers S_1, S_2 and S_3, and d_0 for layers A_1 and A_2, respectively. The quaternary layer has the same lattice constant as InP. Therefore, multiple diffraction takes place for InP and the quaternary layer simultaneously. The diffracted beams suffer absorption when traversing the A_1 and A_2 layers. Their linear absorption coefficient is μ_a. As in the case of a double-layer system, we use, here, the same vectors $\mathbf{T}_l$ and $\mathbf{R}_l$ for forward diffraction, including transmissions and reflections, and vectors $\mathbf{D}_m$ and $\mathbf{X}_m$ for backward diffraction through a layer. Because of the additional layer S_3, the combinations of the reflected beams, m_1 and m_2, from layer S_3 after transmitting through layer

S_2 with those reflected by layer S_2 should be regarded as the new incident beams for layer S_1 for backward diffractions. Similarly, the diffracted beams, l_1 and l_2, of the backward diffractions from layers S_1 and S_2 should be summed up and form the new incident beams for forward diffractions through layer S_3. The block diagram taking these into consideration is shown in Fig. 20. Referring to this diagram, the total reflected powers from the upper surface of S_1, as well as the transmitted ones impinging from the lower surface of S_3, are obtained, after a few manipulations, as

$$\mathbf{P}_M^T(0) = \mathbf{W}_m + \mathbf{X}(d_1)\,\mathbf{M}_1[\mathbf{I}_M - \mathbf{M}_2]^{-1}\,\mathbf{Z}_1 \qquad (26)$$

and

$$\mathbf{P}_L^T(d_1 + d_2 + d_3 + 2d_0) = \mathbf{W}_l + \mathbf{T}(d_3)\,\mathbf{M}_3[\mathbf{I}_L - \mathbf{M}_4]^{-1}\,\mathbf{Z}_2, \qquad (27)$$

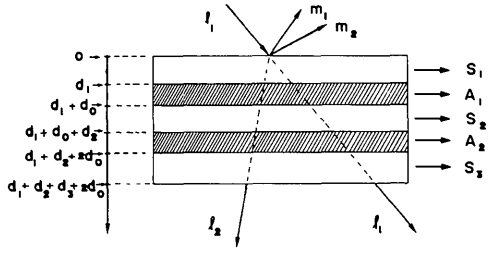

Fig. 19. Multiple diffraction from a triple-layer system.

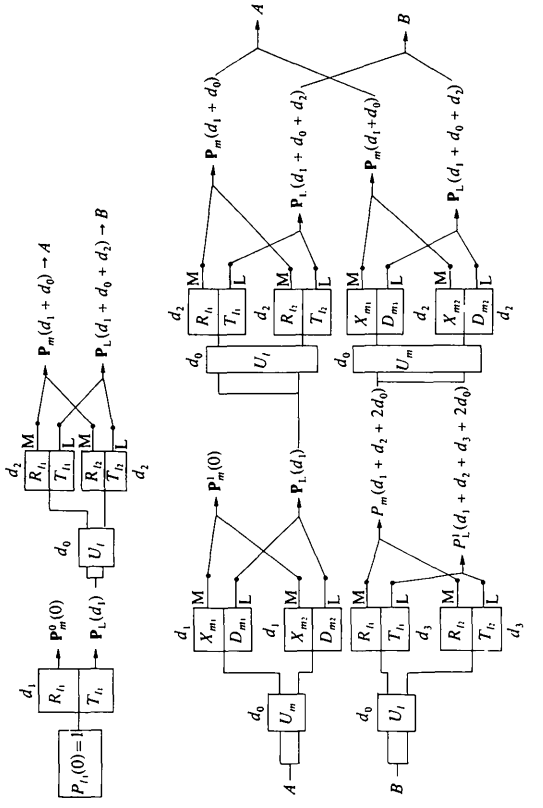

Fig. 20. Block diagram for Fig. 19.

respectively, where

$$\mathbf{W}_m = \mathbf{R}_{l_1}(d_1) + \mathbf{X}(d_1)\,\mathbf{G}(d_2,d_1) + \mathbf{X}(d_1)\,\mathbf{Z}_3(d_3,d_2,d_1)$$

$$\mathbf{W}_l = \mathbf{T}(d_3)\,\mathbf{K}(d_2,d_1) + \mathbf{T}(d_3)\,\mathbf{Z}_4(d_3,d_2,d_1)$$

$$\mathbf{Z}_1 = \begin{bmatrix} \mathbf{Z}_1 \\ \mathbf{Z}_4 \end{bmatrix} \qquad \mathbf{Z}_2 = \begin{bmatrix} \mathbf{Z}_4 \\ \mathbf{Z}_3 \end{bmatrix}$$

$$\mathbf{Z}_3 = \mathbf{F}(d_2,d_1)\,\mathbf{G}(d_2,d_1) + \mathbf{O}(d_2,d_3)\,\mathbf{K}(d_2,d_1)$$

$$\mathbf{Z}_4 = \mathbf{E}(d_2,d_3)\,\mathbf{K}(d_2,d_1) + \mathbf{J}(d_2,d_1)\,\mathbf{G}(d_2,d_1)$$

$$\mathbf{M}_1 = [\mathbf{F}(d_2,d_1) \quad \mathbf{O}(d_2,d_3)]$$

$$\mathbf{M}_2 = \begin{bmatrix} \mathbf{F}(d_2,d_1) & \mathbf{O}(d_2,d_3) \\ \mathbf{J}(d_2,d_1) & \mathbf{E}(d_2,d_3) \end{bmatrix}$$

$$\mathbf{M}_3 = [\mathbf{E}(d_2,d_3) \quad \mathbf{J}(d_2,d_1)]$$

$$\mathbf{M}_4 = \begin{bmatrix} \mathbf{E}(d_2,d_3) & \mathbf{J}(d_2,d_1) \\ \mathbf{O}(d_2,d_3) & \mathbf{F}(d_2,d_1) \end{bmatrix}.$$

The matrices $\mathbf{O}$ and $\mathbf{J}$ and the vector $\mathbf{K}$ are defined as

$$\mathbf{O}(d_2,d_3) = \mathbf{X}_u(d_2)\,\mathbf{R}_u(d_3)$$

$$\mathbf{J}(d_2,d_1) = \mathbf{T}_u(d_2)\,\mathbf{D}_u(d_1)$$

$$\mathbf{K}(d_2,d_1) = \mathbf{T}_u(d_2)\,\mathbf{T}_u(d_1),$$

with

$$\mathbf{T}_u(d) = \begin{bmatrix} u_{l_1}(d_0)\,t_{l_1 m_1}(d) & u_{l_1}(d_0)\,t_{l_1 m_1}(d) \\ u_{l_2}(d_0)\,t_{l_2 m_2}(d) & u_{l_2}(d_0)\,t_{l_2 m_2}(d) \end{bmatrix}.$$

The absorption coefficient μ_a is used for u's. The dimensions are $n_R \times 1$ for $\mathbf{W}_m$, $\mathbf{Z}_3$, $n_T \times 1$ for $\mathbf{W}_l$, $\mathbf{Z}_4$, $(n_R + n_T) \times 1$ for $\mathbf{Z}_1$, $\mathbf{Z}_2$, $(n_R + n_T) \times (n_R + n_T)$ for $\mathbf{M}_2$, $\mathbf{M}_4$, $n_R \times (n_R + n_T)$ for $\mathbf{M}_1$ and $n_T \times (n_R + n_T)$ for $\mathbf{M}_3$. Note that the structure factors of the quaternary layer should be used in calculating the terms involving d_2.

For lattice-matched DH samples, for example 84, (26) and (27), with $d_0 = 0$, were used to obtain the diffracted powers.

References

ANTYPAS, G. A. & MOON, R. L. (1973). *J. Electrochem. Soc.* **120**, 1574–1577.

CATICHA-ELLIS, S. (1969). *Acta Cryst.* A**25**, 666–673.

CHANG, S. L., PATEL, N. B., NANNICHI, Y. & PRINCE, F. C. (1979). *J. Appl. Phys.* **50**, 2975–2976.

COLE, H., CHAMBERS, F. W. & DUNN, H. M. (1962). *Acta Cryst.* **15**, 138–144.

COUSINS, C. S. G., GERWARD, L. & STAUN OLSEN, J. (1978). *Phys. Status Solidi A*, **48**, 113–119.

EVANS, R. C., HIRSCH, P. B. & KELLAR, J. N. (1948). *Acta Cryst.* **1**, 124–129.

HESS, E. (1975). *Z. Kristallogr.* **142**, 305–321.

International Tables for X-ray Crystallography (1968). Vol. III, p. 241. Birmingham: Kynoch Press.
KOSSEL, W. (1936). *Ann. Phys. (Leipzig)*, **26**, 533–553.
MOON, R. M. & SHULL, C. G. (1964). *Acta Cryst.* **17**, 805–812.
NAKAJIMA, K., KUSUNOKI, T., AKITA, K. & KOTANI, T. (1978). *J. Electrochem. Soc.* **125**, 123–127.
OE, K., SHINODA, Y. & SUGIYAMA, K. (1978). *Appl. Phys. Lett.* **33**, 962–964.
PARENTE, C. B. R. & CATICHA-ELLIS, S. (1974). *Jpn. J. Appl. Phys.* **13**, 1501–1505.
POST, B. (1975*a*). In *Anomalous Scattering*, edited by S. RAMASESHAN & S. C. ABRAHAMS, p. 85. Copenhagen: Munksgaard.
POST, B. (1975*b*). *J. Appl. Cryst.* 8, 452–457.
PRAGER, P. R. (1971). *Acta Cryst.* A**27**, 563–569.
RENNINGER, M. (1937). *Z. Phys.* **106**, 141–176.
UNANGST, D. & MELLE, W. (1975). *Acta Cryst.* A**31**, 234–235.
ZACHARIASEN, W. H. (1965). *Acta Cryst.* **18**, 705–710.

Acta Cryst. (1981). A**37**, 889–899

The Influence of Crystal and Sample Symmetries on the Orientation Distribution Function of the Crystallites in Polycrystalline Materials

BY H. J. BUNGE

Institut für Metallkunde und Metallphysik der TU Clausthal, Federal Republic of Germany

C. ESLING

Laboratoire de Métallurgie Structurale, Université de Metz, France

AND J. MULLER

Institut de Mathématiques, Université de Strasbourg, France

(*Received* 24 *February* 1981; *accepted* 7 *May* 1981)

Abstract

In the most general case the orientation distribution of crystals in a polycrystalline sample is to be described by a function of orthogonal transformations which splits up into two functions of rotations corresponding to right- and left-handed crystals. The properties of these functions are influenced by crystal and sample symmetry. The rotational subgroup of crystal symmetry leads to symmetry relations which may be written in the form of selection rules. Elements of the second kind of the crystal symmetry give rise to a determinability condition, according to which the texture function may be split into a part $\tilde{f}(g)$ which can be determined from polycrystal diffraction experiments and a part $\tilde{\tilde{f}}(g)$ which cannot. The determinability condition may take on three different forms according to whether the crystal symmetry contains a centre of inversion, a mirror plane or a $\bar{4}$ inversion axis. In the case of normal scattering the Laue symmetry is to be considered instead of the true crystal symmetry. The sample symmetry is to be described by a black–white or Shubnikov group containing four kinds of elements which give rise to four kinds of symmetry conditions in the function $f(g)$. The sample symmetry may be a conventional one consisting of one-to-one relationships between crystal orientations. It may, however, also be a non-conventional one defined by an integral relation between an infinite number of crystal orientations.

0567-7394/81/060889-11$01.00

1. Introduction

The texture of a polycrystalline material is defined as the orientation distribution function $f(g)$ which describes the orientation density or relative frequency f of crystallites having the orientation g with respect to the sample coordinate system. The crystal orientation g has usually been defined as a *rotation* which brings the sample coordinate system into coincidence with the crystal coordinate system (or *vice versa*).

This definition of crystal orientation is, however, not general enough since it does not allow one to deal with enantiomorphic crystal classes consisting of right- and left-handed crystal forms. But also in the higher symmetric classes this definition is not sufficient in as far as it does not allow one to take symmetry elements of the second kind of the crystal symmetry *correctly* into account, *i.e.* mirror planes, inversion axes, and the centre of symmetry. It is thus necessary to generalize the definition of crystal orientation to orthogonal

© 1981 International Union of Crystallography